Journal of Materials Processing Technology 223 (2015) 284–291

Contents lists available at ScienceDirect

Journal of Materials Processing Technology

journal homepage: www.elsevier.com/locate/jmatprotec

Ti6Al4V titanium alloy welded using concentrated solar energy

A. Romero [b], I. García [a], M.A. Arenas [a,*], V. López [a], A. Vázquez [a]

[a] Surface Engineering, Corrosion and Durability Department, National Center for Metallurgical Research (CENIM-CSIC), Avda. Gregorio del Amo, 8, 28040 Madrid, Spain
[b] Universidad de Castilla-La Mancha, Metallic Materials Group, ETSII-UCLM, Avda. Camilo José Cela s/n, E-13071 Ciudad Real, Spain

ARTICLE INFO

Article history:
Received 29 January 2015
Received in revised form 15 April 2015
Accepted 16 April 2015
Available online 24 April 2015

Keywords:
Titanium alloy
Welding
Concentrated solar energy
Microstructure

ABSTRACT

Sheets of Ti6Al4V titanium alloy in flush corner joint configuration were successfully welded using a 2 kW thermal power vertical axis parabolic concentrator, in a controlled inert argon atmosphere. Longitudinal welds up to 60 mm were performed through controlled displacement of the specimens under the focus of the solar concentrator. After treatments, the welded joints were characterized by microhardness testing and microstructural analysis. Typical microstructures formed at different zones of the welded – melted zone, heat affected zone and base metal – have been identified. Several experimental process parameters have been varied until obtaining a defect-free welded joint. The optimal welding was obtained with solar radiation around 1000 W/m^2 and at 0.15 mm/s constant tracking speed.

1. Introduction

Compared to most structural titanium alloys, Ti6Al4V is considered to be easily weldable and can be welded by a wide variety of conventional fusion processes, such as gas tungsten arc, plasma arc, electron beam or laser.

Gas tungsten arc welding (GTAW), in which the heat of welding is provided by an arc maintained between a nonconsumable tungsten electrode and the workpiece, is the most widely used process for joining titanium sheet. Sunderesan et al. (1999) reported that GTAW permits the obtaining of grain refinement in weld fusion zones for α-β titanium alloys. Balasubramanian et al. (2008) applied GTAW to fabricate joints of Ti6Al4V alloy, showing that not only was there grain refinement but corrosion resistance also improved. The corrosion resistance also increased up to an optimum value with the increase in peak current and pulse frequency.

Plasma arc welding (PAW) is an extension of the GTAW process in which the arc plasma is constricted by a nozzle, thereby increasing its temperature and energy density. A novel dynamically controlled plasma arc welding process was introduced by Chen and Pan (2011) which is able to minimize heat input into the workpiece materials while maintaining desired full penetration and was used to weld Ti6Al4V alloy sheets. Upon comparison with other welds such as GTAW and conventional PAW process, the experimental results revealed improvements including reducing grain size in the fusion zone and better toughness and higher hardness.

Electron beam welding (EBW) involves the melting of the base metals to be joined by the impingement of a focused beam of high-energy electrons. Barreda et al. (2001) compared the use of EBW and PAW processes in plates of Ti6Al4V. PAW welds showed maximum toughness values while EBW welds presented more amounts of martensite α′ phase. Previous investigations, as in the works conducted by Mohandas et al. (1998, 2000), on an α+β titanium alloy, have shown that martensite is a hard but very brittle phase whose presence decreases material toughness. This is the reason why PAW is shown to be a more adequate welding method because this method, as in other arc welding processes, has a higher thermal input and lower cooling rate.

In laser welding (LW), the melting of the workpieces is produced by the impingement of a high-intensity, coherent beam of light. LW method presents a lower heat input that can reduce grain size, but generally has an increased post-weld cooling rate which promotes a martensite transformation, as with the EBW technique. It is therefore necessary to implement a post-weld heat treatment to impart sufficient ductility to affected zones by welding. So, Wang et al. (2010), thus investigated the effect of post-welded heat treatment on the microstructure and mechanical properties of Ti–23Al–17Nb alloy laser beam welding joints. Experimental results revealed that proper post-welded heat treatment improves the ductility of the joint at high temperature.

On the other hand, concentrated solar energy (CSE) has the ability to provide large amounts of energy in small areas, enabling the achievement of high temperatures in very short times and

* Corresponding author. Tel.: +34 915538900; fax: +34 915347425.
E-mail address: geles@cenim.csic.es (M.A. Arenas).

http://dx.doi.org/10.1016/j.jmatprotec.2015.04.015
0924-0136/

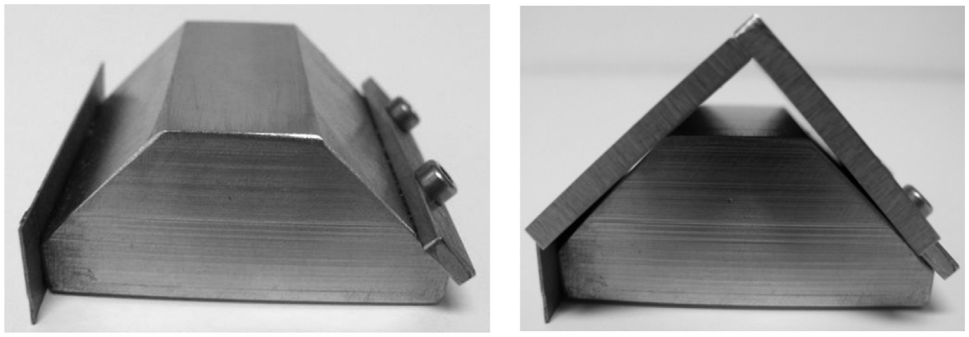

a) b)

Fig. 1. (a) Device used for the correct collocation of the sheets, (b) sheets in flush corner joint configuration placed on the device.

rapid cooling rates that modify diffusion processes. Herranz and Rodriguez (2010) reported that the use of CSE has been researched as an alternative to other types of energy beams for treating and modifying the surfaces of metallic materials. In this line Rodríguez and de Damborenea (1997) carried out surface hardening treatments on 40CrMo4 steel. It was revealed that the hardness value in the quenched zone was approximately 700 HV while in the as-received material it was 250 HV. This surface hardening was obtained in treatment times of less than 30 s. Other treatments using CSE have been made by Herranz et al. (2013, 2014), who carried out the sintering of steel and reinforced steel. These studies were developed successfully and full densities and high mechanical properties were achieved in all cases. Solar investigations using titanium alloys have been focused on treatments such as nitriding in very short times, in pure titanium or Ti6Al4V titanium alloy. Rodríguez et al. (1997) used an arc xenon lamp as a simulator of concentrated solar energy. Results revealed the good quality of the surface nitriding of Ti6Al4V alloy performed in a nitrogen reaction chamber at atmospheric pressure. Sánchez Olías et al. (1999) and Rodríguez et al. (2013) used a Fresnel lens for nitriding by CSE pure titanium and Ti6Al4V, respectively. In both cases, the coatings of TiN obtained were consistent, homogeneous, without pores or defects, and with a uniform thickness throughout the entire sample.

However, solar metal welding literature is scarce and, to the author's knowledge, solar welding of Ti alloy has not been reported. Solar welding of 7075 aluminum alloys was partially achieved by Karalis et al. (2005), but the excessive energy input produced overmelted zones in the welded specimens. Cambronero et al. (2014) employed the CSE to weld aluminum foam plates and several metallurgical joints were obtained on approximately 25 mm thick, even in non-protective atmosphere. Also, Romero et al. (2013) recently conducted welded joints in different geometries by means of CSE. These welded tracks, without defects, were carried out on high melting point metals (H13 tool steel and AISI 316L stainless steel).

This work is focused thus on demonstrating the feasibility of using CSE to weld the Ti6Al4V alloy. Microestructural analysis and micro-hardness measurements will be used to assess the quality of the welded tracks compared to those obtained using other processing techniques.

2. Materials and methods

Ti6Al4V alloy specimens of 30 mm × 60 mm × 5 mm were used. Nominal chemical composition in the as-received condition is given in Table 1.

Specimens were degreased using a commercial soap. Specimens were welded in flush corner joint configuration. All necessary precautions were taken to avoid failed tests and for this reason, an appropriate device was made in AISI 316L stainless steel for this investigation, Fig. 1(a). The joints were made after adequately placing the sheets on such device, as shown in Fig. 1(b).

The specimens were welded in a parabolic solar furnace at the PROMES-CNRS solar facility (Odeillo–Font–Romeu, southeast France). The solar furnace consists of a flat heliostat located on the ground floor that follows the sun and reflects the solar beam towards a parabolic concentrator of 1.5 m diameter and 2 kW of thermal power at the focus, located on the sixth floor (see Fig. 2(a)). The total radiation that it is allowed to pass is controlled by opening or closing the shutter slats. This radiation falls directly on the parabolic mirror that concentrates it onto the focus. The shutter was fully open during the solar welding treatment. Under such conditions, the maximum power density at the focal point (10 mm diameter) is characterized and is approximately 16 MW/m^2.

The specimens placed on the support device were positioned at the focus of the solar system inside a reactor with a quartz chamber, Fig. 2(b). The reactor is provided with a water cooling system. To avoid surface oxidation, an inert argon atmosphere was used in all the welding processes. The atmosphere was maintained in the reactor throughout the test, and additionally for 10 min before and after. The reactor is positioned on a three-axis table which allows placing the piece in the correct position, and also has an automatic motor device allowing carrying out experiments at constant track speeds. Fig. 2(a) shows the situation of the parabolic concentrator and placement of the reactor on top of the three-axis table for conducting the tests. Fig. 2(c) shows the reactor chamber lighting caused by the solar radiation concentrated onto it during the test.

Direct solar irradiance was registered instantaneously with a pyrheliometer mounted on a 2-axis tracking system. The solar radiations registered during the experiments was in the range from 950 to 1000 W/m^2. Due to the impossibility to use thermocouples in the

Table 1
Chemical composition of Ti6Al4V (weight percent, wt%.).

Material	Composition (wt%)								
	Ti	Al	V	Fe	Si	C	N	H	O
Ti6Al4V	Balance	5.5–6.8	3.5–4.5	<0.3	<0.15	<0.1	<0.04	<0.015	<0.15

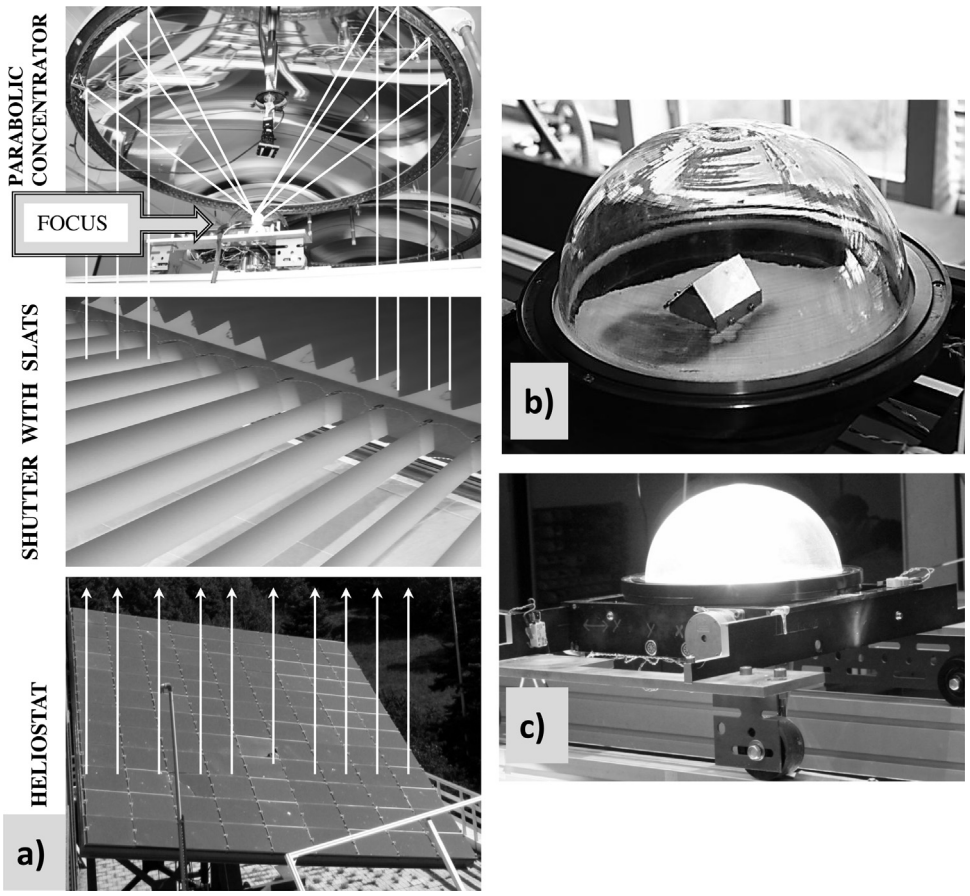

Fig. 2. (a) Diagram showing the solar concentration in the solar furnace in which the flat heliostat, shutter and parabolic concentrator can be seen. (b) Specimens situated inside the quartz chamber reactor. (c) Reactor placed on a three-axis table during a test.

heat affected zones to avoid damage, the melting temperature of Ti6Al4V alloy (around 1660 °C) was assumed as maximum temperature in the melt pool. The solar focus impinged on the area to be welded for sufficient time to melt the material, and a tracking speed was selected at that moment. The tracking speed should be slow enough to melt the material in its path, but fast enough to avoid damages in the welding bead. The determination of the optimal tracking speed for solar welding was done in function of the solar radiation achieved during the experiment. For this reason, all tests were carried out under similar radiation conditions. The tests were performed selecting a tracking speed between 0.15 and 1 mm/s. Several tests were carried out using a constant, or variable tracking speed, up to achieving the full penetration in the entire welded track.

When the welding bead was completely finished, the shutter slats were closed and the piece was cooled inside the reactor under an argon atmosphere with a cooling rate of ~1 °C/s.

Cross sections of the welded samples were prepared and etched with Kroll's reagent (100 mL H_2O, 6 mL HNO_3 and 3 mL HF). The microstructure of the welded samples were analysed by optical microscopy using a NIKON SMZ1500 magnifying glass and OLIMPUS PME3 and OLIMPUS Gx51 optical microscopes. The grain size was determined in the different zones of the welded joint using the test standard ASTM E112-12. This method for measuring average grain size is known as the intercept method and three micrographs from each zone were used to measure the grain size. The intercept method involves an actual count of the number of grains intercepted by a test line or the number of grain boundary intersections with a test line, per unit length of test line, so the mean lineal intercept length can be calculated. Vickers microhardness measurements were carried out on polished cross section surfaces

Table 2
Welding conditions used in the study.

Sample	Tracking speed (mm/s)	Working conditions	Solar insolation (W/m^2)
a	0.6–1	Variable speed	>1000
b	0.15–0.6	Variable speed	1000
c	0.15	Constant speed	950
d	0.15	Constant speed	1000

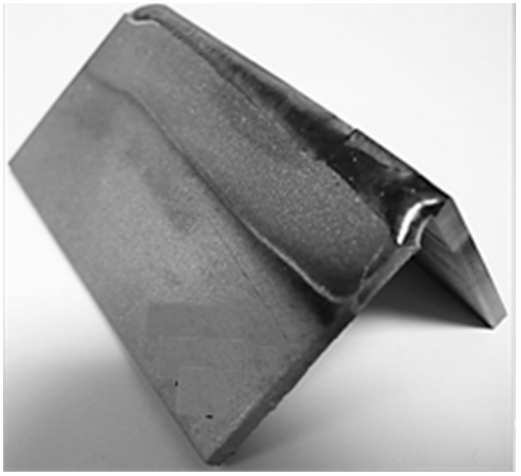

Fig. 3. Example of complete total longitudinal welding of Ti6Al4 V alloy in flush corner joint configuration. (Tracking speed = 0.15 m/s; Solar insolation = 1000 W/m^2).

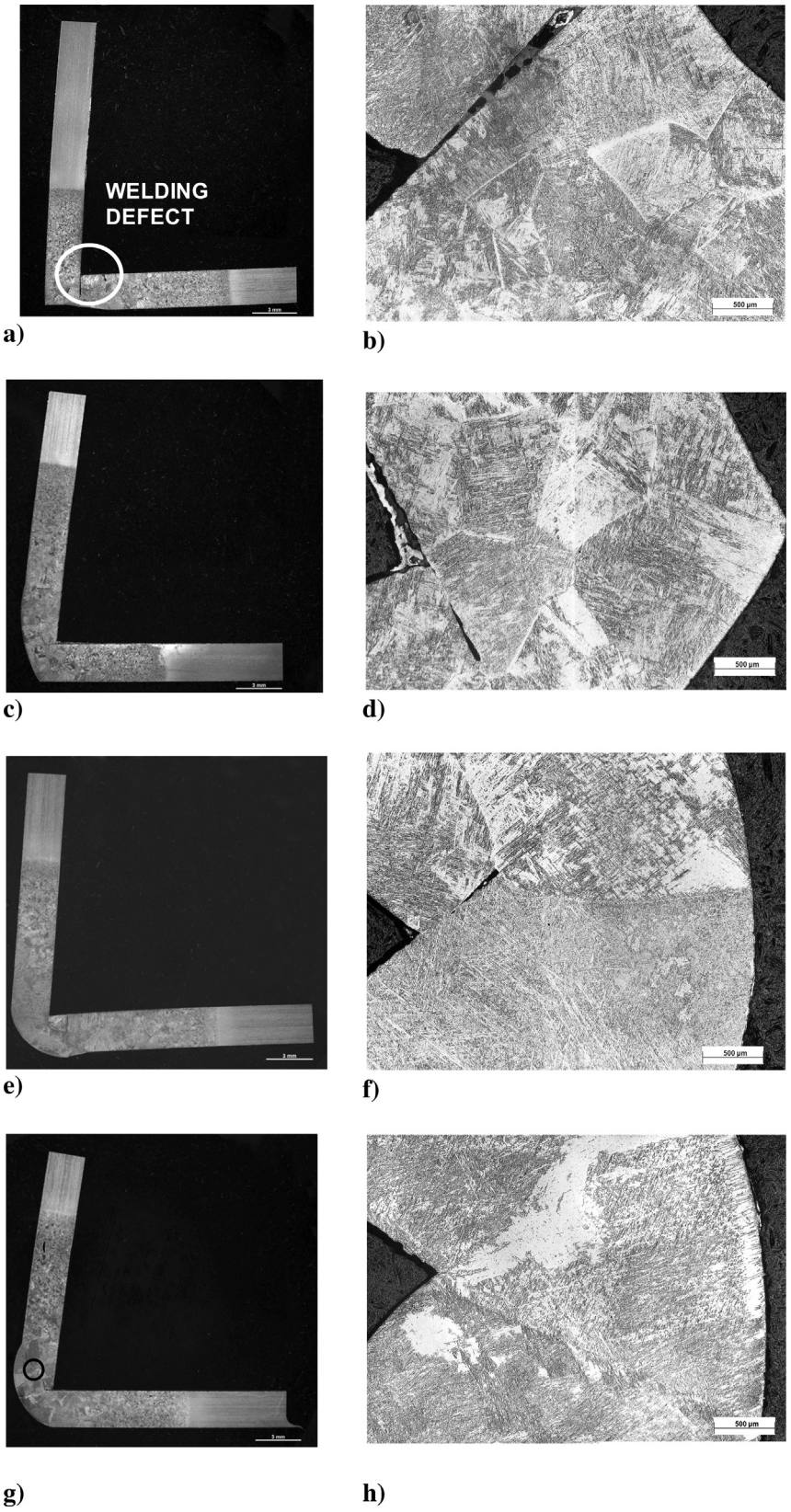

Fig. 4. Macrograph of the cross section of the welded specimens. Sample a (a) and (b). Sample b (c) and (d). Sample c (e) and (f). Sample d (g) zone a = base metal, zone b = heat affected zone, zone c = melted zone; and (h).

using a WILSON WOLPERT microhardness tester, with a load of 300 g (3 N) applied for 10 s ($HV_{0.3}$). The microhardness test has been carried out at 2.5 mm below the surface beginning on the central line of the weld bead.

3. Results and discussion

Visual observation of the weld tracks was carried out on all the specimens during the process. Most of the weld tracks obtained

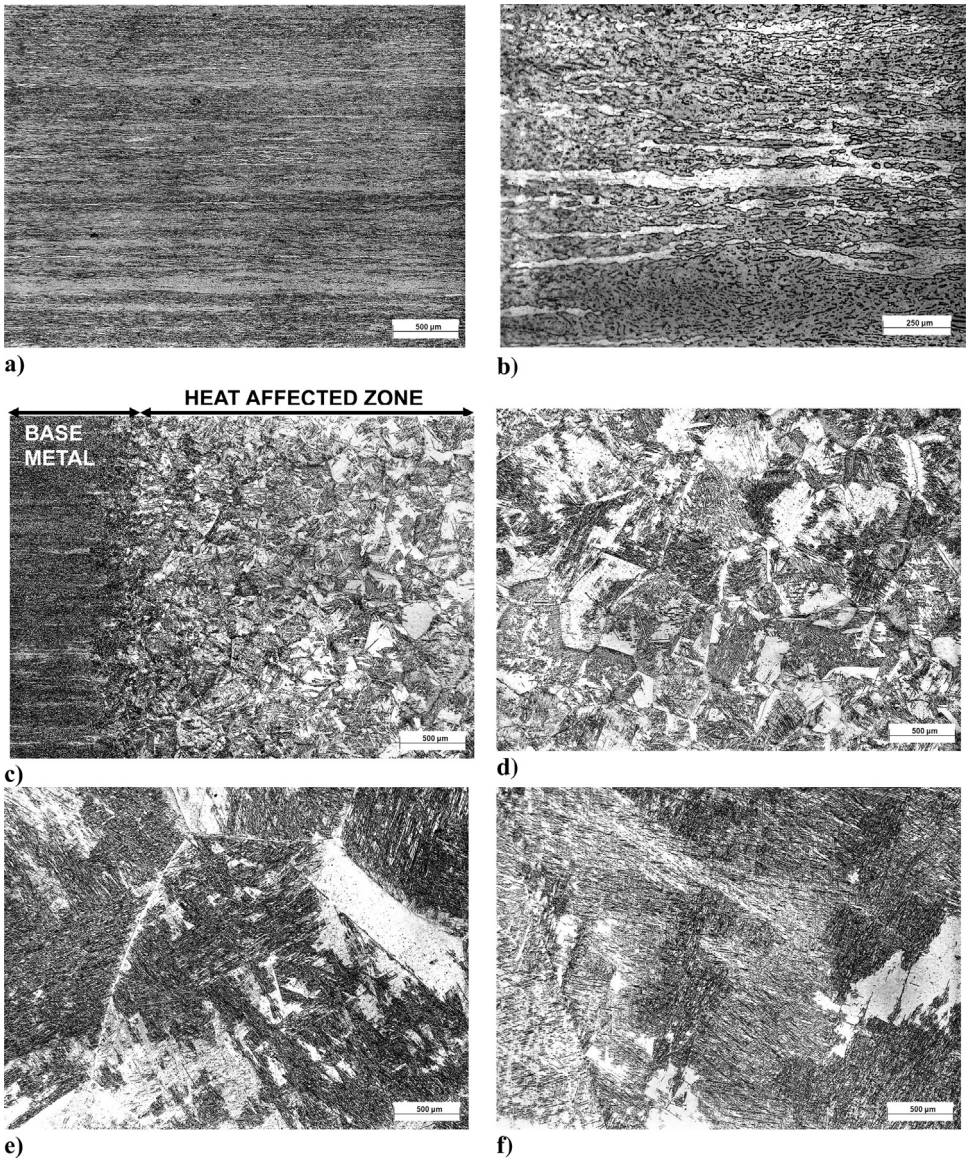

Fig. 5. Microstructure of sample d. Base metal (a) and (b). Transition zone from base material to HAZ (c). HAZ (d) and (e). Melted zone (f).

were completed along the longitudinal extent of the sample and in all cases the welding track surface formed after melting and re-solidification shows a shiny and grey metallic colour, as can be seen in Fig. 3.

Different tracking speeds and solar radiations were selected to determine the best experimental conditions to obtain a complete welding along the thickness of the specimens, since penetration depth is increased with decrease of tracking speed for the same radiation condition.

Table 2 summarizes the experimental conditions used in the present work. In order to investigate the presence of pores, defects or lack of melting, the welded beads were cut perpendicularly to their longitudinal axis and further optical observations were carried out.

The welding was carried out with solar radiation above 1000 W/m^2 for specimen labelled as (a). The tracking speed was initially 0.6 mm/s and was increased to 1 mm/s during the experiment. The welding process lasted 2 min. Welding defects can be observed in the optical observation of the sample (a) using a magnifying glass, Fig. 4(a). At higher magnifications, Fig. 4(b), the lack of melting in the melted zone can be seen along almost the entire thickness of the specimen. The sheets are only joined in the outer part of the welding and the problem appears to be due to the fast tracking speed used during the welding process. The tracking speed was reduced in the sample (b) to increase penetration, so the initial tracking speed was 0.15 mm/s and was increased to 0.6 mm/s when the material started to melt. Defects are not observed using a magnifying glass, Fig. 4(c), but at higher magnifications it can be observed that the weld is not completed, Fig. 4(d).

In specimen (c), a constant and slower tracking speed of 0.15 mm/s was selected during the welding process but the radiation was somewhat lower (above 950 W/m^2). Similarly to that observed in the previous sample, defects are not observed in the macrograph (Fig. 4(e)). However, smaller defects, due to a lack of melting, than in the previous case, can be still seen in the micrograph, Fig. 4(f).

Finally, in sample (d) the welding was carried out using the same tracking speed, 0.15 mm/s, as in sample (c), but the solar radiation increased to 1000 W/m^2. A correct joint between sheets was obtained in this case. Defect-free and complete welding throughout the entire thickness of the sample (d), respectively, can be observed in the macrograph, Fig. 4(g) and micrograph, Fig. 4(h).

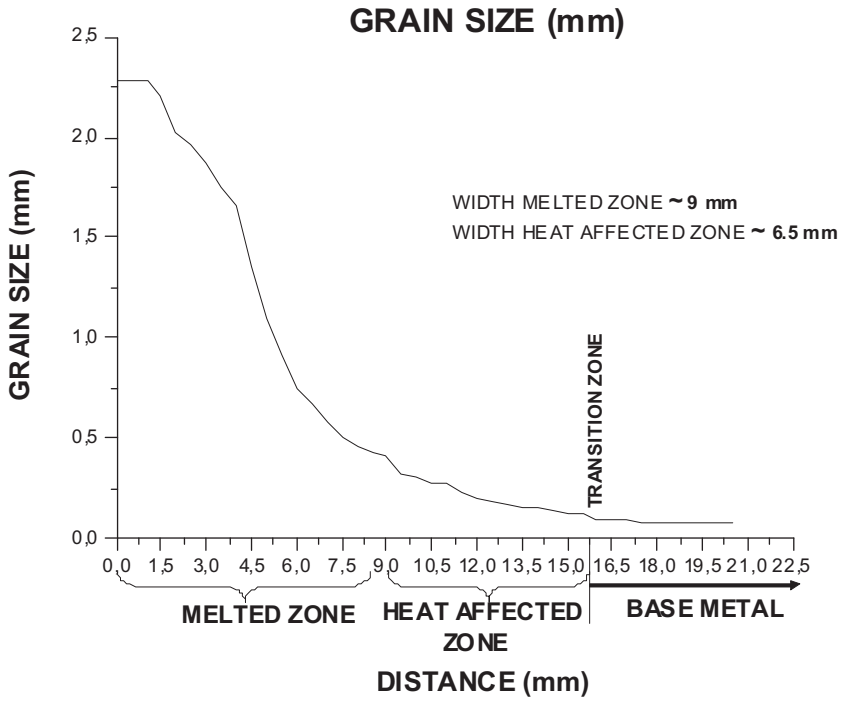

Fig. 6. Grain size distribution in the cross-section of the welded material in function of the distance.

During solar welding, the joint region undergoes a great thermal gradient from the weld pool to the base material; this spatial and temporal distribution of temperature produces a non-uniform microstructure. A metallurgical study was carried out focusing on the microstructure of the different zones of sample (d) because the weld is complete throughout the entire thickness of the specimen and there are not pits, defects or pores. As shown in Fig. 4(g), three different zones are distinguished in the weld: the zone far from the focus is the base metal zone marked as "**a**"; the zone near the focus is the heat affected zone (HAZ) marked as "**b**"; and the zone where the focus impinged is the melted zone (MZ) marked as "**c**".

A more detailed analysis of its microstructure is shown in Fig. 5(a–h). The microstructure of the base metal is shown at different magnifications, Fig. 5(a and b). The microstructure of as-received Ti6Al4V consisted of a phase β (black contrast) distributed at the elongated α (white contrast) grain boundaries. The microstructure is orientated with respect to the rolling direction due to the manufacturing process.

In Fig. 5(c), two completely different microstructures bounded by the transition region from base metal zone to HAZ can be seen. Titanium-base materials have reversible transformation properties that crystal structure changes from an α (hcp, hexagonal close-packed) structure to a β (bcc, body-centered cubic) structure when

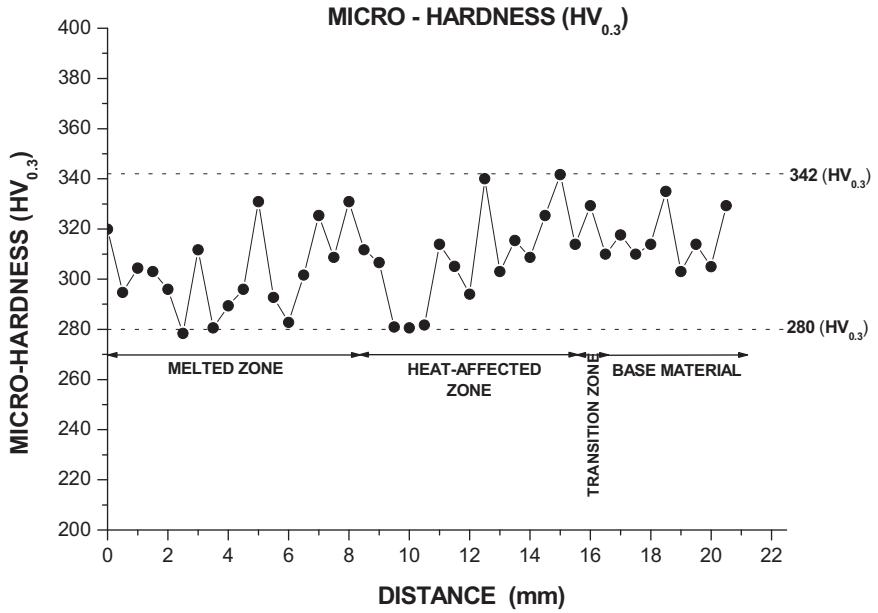

Fig. 7. Hardness profile across the welded joint.

the temperature exceeds to a certain level (β transition temperature). Akman et al. (2009) reported that approximately 995 °C is the value of the β transition temperature in the case of Ti6Al4V alloy.

The microstructure in the HAZ is made up of perfectly defined polygonal α phase grains containing a distinguishable acicular microstructure inside, Fig. 5(d and e).

This acicular, or lamellar, α-phase, namely acicular structure or widmanstätten structure, is the transformation product formed from the β-phase during cooling as there was not enough time for β phase to transform to an α balance phase by diffusion. The absence of martensite indicates that the cooling rate of about 1 °C/s at argon does not allow its formation. Fan et al. (2005) and Gao et al. (2013) found a similar result during investigations of Ti6Al4V welding using other techniques. The welds were made by laser and by TIG, respectively.

A different size grain in the HAZ can be seen. The HAZ close to the base material, Fig. 5(d), presents a smaller size grain than in the HAZ far from base material, Fig. 5(e). The significant differences found in HAZ were due to the different temperatures achieved along this zone, so the temperature achieved in HAZ close to the base material was the lowest temperature above the β transition temperature and, consequently, the grain size was smaller. The HAZ far from base material contained a large number of acicular α-phase and a larger size grain due to the relative high temperature in the thermal cycle process. The acicular α microstructure can be also seen in the micrograph of the melted zone, Fig. 5(f), where the largest grain sizes have obviously been obtained due to the highest temperatures reached in this zone.

These results can be compared with findings reported by other authors. Akman et al. (2009) and Zhao et al. (2011) studied the microstructural features obtained in Ti6Al4Al by laser welding using a Nd:YAG laser. In the case of the study presented by Akman et al. (2009), the high cooling rates also caused the formation of martensite in the weld zone. This phenomenon is also similar to other results reported recently by Gao et al. (2013) who carried out a comparative study between the welding process of the Ti6Al4V alloy using a pulsed Nd:YAG laser beam and a gas tungsten arc (TIG). The differences obtained were very revealing. In the case of laser beam welding, the cooling rate was always above the critical cooling rate of 410 °C/s which allowed the formation of a full martensite, while at lower cooling rates the transformation was preferential to forming more orderly acicular α-phase at prior β grain boundaries.

These same phases (martensite and acicular α-phase) obtained at different cooling rates in the α+β alloys were reported by Ahmed and Rack (1998) who analyzed the phase transformations during cooling in the Ti6Al4V alloy.

Moreover, the depth of the weld is determined using the optical microscope and it is approximately 15.5 mm long (9 mm in melted zone and 6.5 mm in HAZ), the remaining the length of the sample, up to 30 mm, corresponds to base material zone (14.5 mm).

The grain size was determined using the intercept method. As gathered in Fig. 6, the grain size increases with the decrease of the distance to the weld centreline in both the HAZ and melted zone. This is due to the heat-input increases at shorter distances to the focal point. The range of grain size is between 2.28 mm to 0.43 mm in melted zone, between 0.43 mm to 0.13 mm in heat affected zone and between 0.13 mm to 0.10 mm in transition zone. The increasing of the grain size is much greater than that obtained using other techniques such as laser welding as it was reported by Akman et al. (2009) where the maximum grain size was 0.35 mm in the melted zone.

The microhardness test has been carried out at 2.5 mm below the surface beginning on the central line of the weld bead, as already mentioned. The hardness values have been measured every 0.5 mm from the melted zone to the base material zone. The hardness distribution in the cross-section of the welded material as a function of the distance to focus is depicted in Fig. 7. The microhardness value is around 315 ± 11 HV in the base material, this value is similar to that obtained by Squillace et al. (2012) for sheets of Ti6Al4V in similar as-received conditions. Moreover, the average microhardness values are around 309 ± 20 HV and 303 ± 16 HV in the HAZ and melted zones, respectively. A slightly softening trend from the base material to the melted zone is observed but is not statistically significant due to the high dispersion in the data. These values and scatter are similar to other results presented by Chen and Pan (2011) for a commercial Ti6Al4V alloy plate. In this case, the dynamically controlled PAW, GTAW and regular keyhole PAW were selected to make comparative welds. In all cases, the variation of the microhardness value was relatively large and the microhardness values were between 310 and 385 HV depending on the welding technique. Moreover, microhardness differences were not found in the different welding zones, as in the present study. The average hardness value of the dynamically controlled PAW joint was slightly higher than that of the keyhole PAW and GTAW joints, presumably because of the higher cooling rate which may be expected to induce a slightly greater amount of martensite.

4. Conclusions

This work demonstrated the possibility to obtain Ti6Al4V alloy welded joints by concentrated solar energy. The following conclusions were drawn:

- 5 mm thick Ti6Al4V alloy sheets were welded in flush corner joint configuration.
- A full penetration of welded tracks without defects was obtained with a tracking speed of 0.15 mm/s and a solar radiation of 1000 W/cm^2.
- The absence of martensite in the microstructure indicates that the cooling rate at argon (about 1 °C/s) is not fast enough. Consequently, a more orderly acicular α-phase is presented both in the heat affected zone of 6.5 mm wide as well as in the 9 mm wide melted zone.
- The microhardnes is very similar throughout the entire welded piece (around 310 HV) and is similar to that found in the as-received material, despite the large increase in the grain size in the heat affected zones.

Acknowledgements

This work was supported by the Access to Research Infrastructures Activity in the 7th Framework Program of the EU (SFERA Grant Agreement no. 228296) as well as the use of the facilities and its researchers/technology experts at the PROMES–CNRS Solar facility, and by the Spanish National Program (Project “SMOTI”, MAT2009-13571).

References

Ahmed, T., Rack, H.J., 1998. Phase transformations during cooling in α+β titanium alloys. Mater. Sci. Eng., A 243, 206–211.

Akman, E., Demir, A., Canel, T., Sinmazçelik, T., 2009. Laser welding of Ti6Al4V titanium alloys. J. Mater. Process. Technol. 209, 3705–3713.

Balasubramanian, M., Jayabalan, V., Balasubramanian, V., 2008. Effect of pulsed gas tungsten arc welding on corrosion behavior of Ti-6Al-4V titanium alloy. Mater. Des. 29, 1359–1363.

Barreda, J.L., Santamaría, F., Azpiroz, X., Irisarri, A.M., Varona, J.M., 2001. Electrom beam welded high thickness Ti6Al4V plates using filler metal of similar and different composition to the base plate. Vacuum 62, 143–150.

Cambronero, L.E.G., Cañadas, I., Ruiz-Román, J.M., Cisneros, M., Corpas Iglesias, F.A., 2014. Weld structure of joined aluminium foams with concentrated solar energy. J. Mater. Process. Technol. 214 (11), 2637–2643.

Chen, Jian-chun, Pan, Chun-xu, 2011. Welding of Ti–6Al–4V alloy using dynamically controlled plasma arc welding process. Trans. Nonferrous Met. Soc. China 2, 1506–1512.

Fan, Y., Cheng, P., Yao, Y.L., Yang, Z., Egland, K., 2005. Effect of phase transformations on laser forming of Ti–6Al–4V alloy. J. Appl. Phys. 98, 1 (art. no. 013518).

Gao, Xiao-Long, Zhang, Lin-Jie, Liu, Jing, Zhang, Jian-Xun, 2013. A comparative study of pulsed Nd:YAG laser welding and TIG welding of thin Ti6Al4V titanium alloy plate. Mater. Sci. Eng., A 559, 14–21.

Herranz, G., Rodriguez, G.P., 2010. Uses of concentrated solar energy in materials science. In: Rugescu, R.D (Ed.), Solar Energy. InTech, Croatia, pp. 145–170.

Herranz, G., Romero, A., De Castro, V., Rodríguez, G.P., 2013. Development of high speed steel sintered using concentrated solar energy. J. Mater. Process. Technol. 213 (12), 2065–2073.

Herranz, G., Romero, A., De Castro, V., Rodríguez, G.P., 2014. Processing of AISI M2 high speed steel reinforced with vanadium carbide by solar sintering. Mater. Des. 54, 934–946.

Karalis, D.G., Pantelis, D.I., Papazoglou, V.J., 2005. On the investigation of 7075 aluminum alloy welding using concentrated solar energy. Sol. Energy Mater. Sol. Cells 86, 145–163.

Mohandas, T., Banerjee, D., Kutumba Rao, V.V., 1998. Observations on impact toughness of electron beam welds of an α+β titanium alloy. Mater. Sci. Eng., A 254, 147–154.

Mohandas, T., Bajerjee, D., Kutumba Rao, V.V., 2000. Microstructure and mechanical properties of friction welds of an α+β titanium alloy. Mater. Sci. Eng., A 289, 70–82.

Rodríguez, G.P., de Damborenea, J.J., Vázquez, A.J., 1997. Surface hardening of steel in a solar furnace. Surf. Coat. Technol. 92, 65–170.

Rodríguez, C., García, I., de Damborenea, J.J., Vázquez, A.J., 1997. Characterisation of an arc xenon lamp and its application to titanium nitride synthesis. Sol. Energy Mater. Sol. Cells 45 (2), 185–197.

Rodríguez, G.P., Herranz, G., Romero, A., 2013. Solar gas nitriding of Ti6Al4V alloy. Appl. Surf. Sci. 283, 445–452.

Romero, A., García, I., Arenas, M.A., López, V., Vázquez, A., 2013. High melting point metals welding by concentrated solar energy. Sol. Energy 95, 131–143.

Sánchez Olías, J., García, I., Vázquez, A.J., 1999. Synthesis of TiN with solar energy concentrated by a Fresnel lens. Mater. Lett. 38 (5), 379–385.

Squillace, A., Prisco, U., Ciliberto, S., Astarita, A., 2012. Effect of welding parameters on morphology and mechanical properties of Ti–6Al–4V laser beam welded butt joints. J. Mater. Process. Technol. 212, 427–436.

Sunderesan, S., Janaki Ram, G.D., Madhusudhan Reddy, G., 1999. Microstructural refinement of weld fusion zones in α-β titanium alloys using pulsed current welding. Mater. Sci. Eng., A 262, 88–100.

Wang, Guo-qing, Wu, Ai-ping, Zhao, Yue, Zou, Gui-sheng, Chen, Qiang, Ren, Jia-lie, 2010. Effect of post-weld heat treatment on microstructure and properties of Ti–23Al–17Nb alloy laser beam welding joints. Trans. Nonferrous Met. Soc. China 20 (5), 732–739.

Zhao, Shusen, Yu, Gang, He, Xiuli, Zhang, Yongjie, Ning, Weijian, 2011. Numerical simulation and experimental investigation of laser overlap welding of Ti6Al4V and 42CrMo. J. Mater. Process. Technol. 211, 530–537.